M-current inhibition rapidly induces a unique CK2-dependent plasticity of the axon initial segment

Jonathan Lezmy[a,b], Maya Lipinsky[a,b], Yana Khrapunsky[c,d], Eti Patrich[a,b], Lia Shalom[a,b], Asher Peretz[a,b], Ilya A. Fleidervish[c,d,1], and Bernard Attali[a,b,1]

[a]Department of Physiology and Pharmacology, Sackler Faculty of Medicine, Tel Aviv University, Tel Aviv 69978, Israel; [b]Sagol School of Neuroscience, Tel Aviv University, Tel Aviv 69978, Israel; [c]Department of Physiology and Cell Biology, Faculty of Health Sciences, Ben-Gurion University of the Negev, Beer Sheva 84105, Israel; and [d]Zlotowski Center for Neuroscience, Faculty of Health Sciences, Ben-Gurion University of the Negev, Beer Sheva 84105, Israel

Edited by Lily Yeh Jan, University of California, San Francisco, CA, and approved October 20, 2017 (received for review May 25, 2017)

Alterations in synaptic input, persisting for hours to days, elicit homeostatic plastic changes in the axon initial segment (AIS), which is pivotal for spike generation. Here, in hippocampal pyramidal neurons of both primary cultures and slices, we triggered a unique form of AIS plasticity by selectively targeting M-type K^+ channels, which predominantly localize to the AIS and are essential for tuning neuronal excitability. While acute M-current inhibition via cholinergic activation or direct channel block made neurons more excitable, minutes to hours of sustained M-current depression resulted in a gradual reduction in intrinsic excitability. Dual soma–axon patch-clamp recordings combined with axonal Na^+ imaging and immunocytochemistry revealed that these compensatory alterations were associated with a distal shift of the spike trigger zone and distal relocation of FGF14, Na^+, and K_v7 channels but not ankyrin G. The concomitant distal redistribution of FGF14 together with Na_v and K_v7 segments along the AIS suggests that these channels relocate as a structural and functional unit. These fast homeostatic changes were independent of L-type Ca^{2+} channel activity but were contingent on the crucial AIS protein, protein kinase CK2. Using compartmental simulations, we examined the effects of varying the AIS position relative to the soma and found that AIS distal relocation of both Na_v and K_v7 channels elicited a decrease in neuronal excitability. Thus, alterations in M-channel activity rapidly trigger unique AIS plasticity to stabilize network excitability.

homeostatic plasticity | axon initial segment | M-current | potassium channel | K_v7

Neurons use a variety of homeostatic mechanisms to stabilize ongoing network activity in the face of bidirectional input perturbations that cause firing rates to deviate from a defined set point (1). The adaptive mechanisms include synaptic scaling, changes in the number of synapses or dendritic excitability (2–6), and structural and functional alterations of the axon initial segment (AIS) (7–13).

Strategically situated between the somatodendritic and axonal compartments, the AIS spans the proximal unmyelinated part of the axon (10–60 μm) to trigger and shape action potentials (APs) and to determine neuronal output (7–13). The AIS provides a diffusion barrier that restricts membrane protein motion and lipids exchange and serves as a filter that selectively excludes somatodendritic vesicles and recruits axonal cargoes (14–16). The structural architecture of the AIS consists of ion channels and cell-adhesion molecules anchored to specialized cytoskeletal protein scaffolds, ankyrin G and βIV spectrin, that are connected to actin filaments and microtubules (7, 12, 13, 15, 17, 18). Actin rings are regularly found (at a 190-nm period) along the AIS and distal axon (17, 18). Ankyrin G binds subtypes of voltage-gated sodium (Na_v) and potassium (K_v) channels via a specific analogous motif, ensuring their clustering at the AIS (19–22). In mature neurons of the cortex and hippocampus, $Na_v1.2$ preferentially localizes to the proximal part of the AIS, while $Na_v1.6$ and $K_v7.2/K_v7.3$ cluster along the distal part (12, 23, 24). The lower activation threshold of $Na_v1.6$ channels compared with $Na_v1.2$, their segregation from the soma, and their distal AIS location make them suitable for AP generation (12, 23). Assembled as heterotetramers of $K_v7.2$ and $K_v7.3$ subunits, M-channels produce a low-threshold, slowly activating and non-inactivating K^+ current modulated by cholinergic muscarinic agonists (25, 26). The recently reported M-current density gradient toward the AIS distal end led to the proposal that $K_v7.2/3$ channels exert stabilizing effects on the resting membrane potential, which prevents subthreshold potential activation of persistent Na^+ current and restrains spontaneous firing but also increases the availability of Na^+ channels (27).

Long considered to be the trigger zone for AP initiation (28), the AIS was regarded as a static and rigid structure encompassing ion channels anchored to a scaffolding and cytoskeletal protein network. Now, it is recognized that the AIS is a highly dynamic structure, capable of structural and functional plasticity and continuously adapting to changes in neuronal activity (8, 12, 29–31). In 2010, two seminal studies found that changes in neuronal activity could lead to AIS relocation or resizing as a new mechanism of slow homeostatic adaptation (32, 33). Auditory input deprivation for 3–7 d led to AIS elongation associated with enhanced excitability in nucleus magnocellularis neurons of chicken (33). Conversely, in cultured hippocampal neurons, increase in neuronal activity for 2 d by optogenetic stimulation or by high-K^+–induced depolarization resulted in distal relocation of the AIS, which correlated with a decrease in excitability (32). In hippocampal dentate granule cells, the same depolarizing trigger applied for only 3 h caused two main alterations that counteracted each other,

Significance

The axon initial segment (AIS), the region where neurons generate spikes, was recently shown to be a highly dynamic structure, exhibiting plasticity over wide timescales. Here we triggered a unique form of AIS plasticity in hippocampal pyramidal neurons by selectively targeting the AIS M-type K^+ channels. We uncovered the mechanisms whereby sustained cholinergic activation or direct M-channel block rapidly trigger a unique form of AIS plasticity. Minutes to hours of sustained M-current depression resulted in a compensatory reduction in intrinsic excitability associated with distal shift of the axonal spike trigger zone and distal relocation of both Na^+ and M-channels. These fast homeostatic changes, necessary to stabilize network excitability, were dependent on the crucial AIS protein, protein kinase CK2.

Author contributions: J.L., I.A.F., and B.A. designed research; J.L., M.L., Y.K., E.P., L.S., A.P., and I.A.F. performed research; I.A.F. contributed new reagents/analytic tools; J.L., M.L., Y.K., E.P., L.S., A.P., I.A.F., and B.A. analyzed data; and I.A.F. and B.A. wrote the paper.

The authors declare no conflict of interest.

This article is a PNAS Direct Submission.

Published under the PNAS license.

[1]To whom correspondence may be addressed. Email: ilya@bgu.ac.il or battali@post.tau.ac.il.

This article contains supporting information online at www.pnas.org/lookup/suppl/doi:10.1073/pnas.1708700114/-/DCSupplemental.

shortening of the AIS and dephosphorylation of Na^+ channels, thereby maintaining the excitability at a similar level (34).

Here we triggered plasticity by selectively targeting the M-channels, which are integral components of the AIS (21) and are fine tuners of neuronal excitability (25, 35, 36). We applied either the selective M-channel blocker XE-991 or the cholinergic muscarinic agonist carbachol, which via the Gq protein-coupled muscarinic receptors–phospholipase C cascade causes the breakdown of phosphatidylinositol-4,5-bisphosphate, thereby destabilizing the M-channel open state and inhibiting the M-current (37). Acute M-current inhibition by carbachol or by XE-991 increased the intrinsic excitability of cultured hippocampal pyramidal neurons as well as hippocampal network activity. This effect was transient, however. Hippocampal neurons subjected to M-current inhibition for extended periods of more than 1 h showed a gradual decrease in intrinsic excitability associated with a distal shift in the spike trigger zone and a relocation away from the soma of the FGF14, Na_v, and $K_v7.3$ channels but not of ankyrin G. Similar results were obtained in CA1 pyramidal neurons of acute hippocampal slices. The functional and structural plastic changes in the AIS induced by M-channel blockage were insensitive to L-type Ca^{2+} channel activity but were dependent on protein kinase CK2, which plays a central role in AIS function. Hence, perturbation of M-channel activity produces a rapid and unique form of homeostatic plasticity to stabilize neuronal excitability.

Results

M-Channel Inhibition Triggers Fast Homeostatic Changes in Intrinsic Excitability of Cultured Hippocampal Neurons. Whole-cell patch-clamp recording was first performed on cultured hippocampal neurons with pyramidal-like morphology [14–16 d in vitro (DIV)]. Acute exposure of cells to 10 μM carbachol or 10 μM XE991 resulted in the inhibition of 62% and 70% of the M-current, respectively, which significantly depolarized the resting membrane potential (ΔV = +2.1 mV and ΔV = +5.9 mV, respectively) and increased the spontaneous firing rate (4.1-fold and 1.9-fold, respectively) (Fig. 1*A* and Figs. S1 *A* and *B* and S2 *A* and *B*). M-current blockage by XE-991 was maintained at the same level when neurons were chronically exposed to the drug for extended periods of 1–48 h (Fig. 1*A*). The increase in the spontaneous firing rate was still significant following 1–4 h of XE991 chronic treatment and was comparable to that observed after acute M-channel inhibition. For longer time exposures (24 and 48 h), the spontaneous firing rate decreased progressively and returned to the values of untreated neurons (Fig. S1*B*), reflecting a slow adaptation and suggesting the involvement of slow homeostatic plasticity processes (1). XE991 was stable during prolonged incubation conditions, as shown by a significant increase in the spontaneous firing rate (2.1-fold) following acute exposure of naive hippocampal neurons (formerly incubated for 48 h with a hippocampal culture) to a XE991 solution (10 μM) (Fig. S1*C*).

We focused our study on homeostatic changes in intrinsic excitability induced by M-current inhibition. Therefore recordings were performed in the presence of synaptic receptor blockers in the extracellular solution. As expected, acute bath application of the cholinergic agonist carbachol (10 μM) or the M-channel blocker XE991 (10 μM) significantly altered the intrinsic characteristics of hippocampal neurons, decreasing threshold current and AP amplitude, increasing AP width, apparent input resistance, and frequency of evoked spike discharge, and depolarizing resting membrane potential (RMP) (Fig. 1 *B–D* and Figs. S2 *B* and *C* and S3*A*). Sustained cholinergic activation by carbachol or M-current block by XE991 led to rapid adaptive changes (after 1–4 h) that progressively brought these values back to those of untreated neurons. For example, after 1 h of carbachol or XE-991 exposure, the threshold current and the frequency of evoked spike discharge almost completely returned to the pretreatment values (Fig. 1 *B–D* and Figs. S2 *B* and *C* and S3*A*). As shown above, this rapid homeostatic outcome was not the result of increased M-current density (Fig. 1*A*). Thus, the results indicate that sustained M-channel inhibition resulting from either cholinergic muscarinic activation or direct channel block induced rapid adaptive changes in the intrinsic excitability of hippocampal neurons and that this 1-h timescale of compensation is faster than that of the

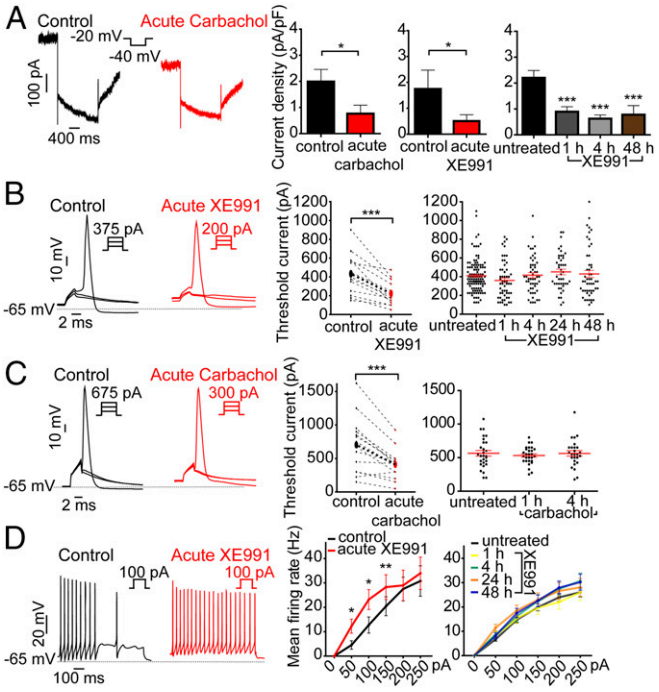

Fig. 1. M-current inhibition by carbachol or XE991 triggers fast homeostatic changes in the intrinsic excitability of cultured hippocampal neurons. (*A*) Representative M-currents, measured by the standard deactivation protocol (holding at −20 mV and deactivation at −40 mV), were inhibited following acute and prolonged exposure to 10 μM carbachol or 10 μM XE991, as indicated. M-currents were significantly inhibited by acute carbachol exposure (two-tailed paired *t* test: $*P = 0.0271$; $t = 2.835$ df = 15, $n = 16$). M-currents were significantly inhibited by acute XE991 exposure (two-tailed paired *t* test: $*P = 0.0125$; $t = 2.450$, df = 15, $n = 16$). M-currents were significantly inhibited by chronic XE991 treatment [one-way ANOVA: $P < 0.001$, F = 8.602, df = 3, and post hoc Tukey's multiple comparison test: significantly different ($***P < 0.001$) for untreated ($n = 49$) vs. 1 h ($n = 46$), untreated vs. 4 h ($n = 47$), and untreated vs. 48 h ($n = 42$)]. (*B*) Representative traces of solitary spike discharge evoked by 2-ms step injection of depolarizing currents with increments of 25 pA to measure the threshold current in the absence or presence of 10 μM XE991. Acute XE991 exposure significantly decreased the threshold current (two-tailed paired *t* test: $***P < 0.0001$; $t = 5.841$, df = 13, $n = 14$). In chronic XE991 treatment, the threshold currents in untreated ($n = 113$), 1 h ($n = 55$), 4 h ($n = 52$), 24-h XE991 treatment ($n = 44$), and 48 h ($n = 51$) were not significantly different (one-way ANOVA, $P = 0.2228$; F = 1.433, df = 4). (*C*) Representative traces of solitary spike discharge evoked by 2-ms step injection of depolarizing currents with increments of 25 pA in the presence of synaptic blockers to measure the threshold current in the absence or presence of 10 μM carbachol. Acute carbachol exposure significantly decreased the threshold current (two-tailed paired *t* test: $***P = 0003$; $t = 4.922$, df = 13, $n = 14$). In chronic carbachol treatment, the threshold currents in untreated ($n = 28$), 1 h ($n = 28$), and 4 h ($n = 26$) were not significantly different (one-way ANOVA, $P = 0.7684$, F = 0.2643, df = 2). (*D*) Representative spike discharge evoked by 800-ms step injection of depolarizing current with increments of 50 pA in the presence of synaptic blockers to measure the rate of discharge. Acute XE991 treatment significantly increases the rate of evoked spike discharge [two-tailed paired *t* test: 50 pA, $*P = 0.014$, $t = -2.985$, df = 10; 100 pA, $*P = 0.017$, $t = -2.863$, df = 10; 150 pA, $**P = 0.007$, $t = -3.348$, df = 10; 200 pA, $P = 0.651$, $t = -0.467$, df = 10; 250 pA, $P = 0.311$, $t = -1.068$, df = 10 ($n = 11$)]. In chronic XE991 treatment, the rates of spike discharge were not significantly different: untreated: $n = 102$; 1 h: $n = 39$; 4 h: $n = 40$; 24 -h: $n = 37$; 48 h: $n = 46$; repeated measures ANOVA, $P = 0.916$, F = 0.171, df = 3.

homeostatic alterations in the spontaneous firing rate, which take 1–2 d to occur.

M-Channel Inhibition Triggers a Rapid Distal Redistribution of AIS Na_v and $K_v7.3$ Channels Followed by a Slow Distal Relocation of Ankyrin G. Staining for ankyrin G, Na_v channels, and $K_v7.3$ K^+ channels was performed in cultured hippocampal neurons (16 DIV) with selective antibodies. In control conditions, the proximal boundaries of ankyrin G, $K_v7.3$, and Na_v immunofluorescence were found at approximately the same location in the AIS, while the distal boundary of the $K_v7.3$ label was consistently more proximal than that of ankyrin G and Na_v (Fig. 2 *A*–*C*). In addition, the ankyrin G stain extended slightly farther than that of Na_v. A distal shift in the start of $K_v7.3$ and Na_v channel labels became evident after 1-h incubation with 10 μM XE991. The distance between the soma and the proximal boundary of both $K_v7.3$ and Na_v immune signals increased progressively, reaching steady values of 3.9 ± 0.8 μm (untreated: $n = 133$; XE991-treated: $n = 111$) and 4.9 ± 1.3 μm (untreated: $n = 99$; XE991-treated: $n = 91$), respectively, after 4 h of XE991 exposure (Fig. 2 *A*–*C*). The extent of this distal relocation away from the soma remained the same after longer XE991 incubation for up to 2 d. A similar distal shift was observed for the end label of $K_v7.3$ and Na_v immunofluorescence, such that the total length of $K_v7.3$ and Na_v channel distributions in the AIS remained the same throughout the XE991 treatment (Fig. 2 *A* and *B*). When Na_v channels were costained with anti-MAP2 antibodies, a similar distal shift of the Na_v immune signal, 4.6 ± 0.8 μm, was found after 4 h of XE991 treatment (untreated: $n = 64$; XE991-treated: $n = 61$) (Fig. S4). Also, no significant differences in $K_v7.3$ and Na_v immunofluorescence intensities were observed as determined by the AIS channel:soma or AIS channel:ankyrin G intensity ratios (Fig. S3*B*). Bath application of the muscarinic agonist carbachol elicited a similar effect on the distribution of the AIS channels. Thus, exposure of the neurons to carbachol for 4 h promoted a distal shift of the $K_v7.3$ immune signal by 4.6 ± 0.9 μm (untreated: $n = 54$; XE991-treated: $n = 51$) (Fig. 2*E*). To investigate whether the distal channel redistribution was bidirectional, hippocampal neurons (14 DIV) were incubated for 4 h with 10 μM XE991, which subsequently was washed out for 24 h. Immunostaining performed following the washout of XE991 revealed that the total length and the distance between the start of the $K_v7.3$ segment and the soma was similar to that of untreated neurons, indicating that the distal shift of the channels was reversible (Fig. 2*D*).

A recent study showed that FGF14 physically interacts with both the $Na_v1.6$ and $K_v7.2$ channels, thereby enabling their bridging in the AIS. FGF14 was proposed to be an organizer of $Na_v1.6$ and K_v7 channel localization in the AIS, suggesting their coordinated function (38). If this is indeed the case, one should expect that FGF14 would follow similar homeostatic changes after extended M-channel inhibition. In agreement with this idea, FGF14 immunostaining exhibited a significant 4-μm distal shift after 4 h of XE991 treatment without a change in its total length (Fig. S5). This FGF14 distal relocation is like that of the $K_v7.3$ and Na_v channels. In line with previous work (38, 39), the length of the FGF14 label was shorter than that of ankyrin G (~24 μm versus 33 μm) (Fig. 2*C* and Fig. S5).

In contrast to the $K_v7.3$ and Na_v channels, the ankyrin G label did not exhibit a distal shift from the soma following a 4-h XE991 treatment. Only after 2 d of XE991 exposure did an ankyrin G distal relocation of about 3.9 ± 1.4 μm occur (untreated: $n = 91$; XE991-treated for 48 h: $n = 99$). The extent of the ankyrin G distal shift was similar to that found for the $K_v7.3$ and Na_v channels. However, the total length of the ankyrin G platform did not change throughout the chronic XE-991 exposure and remained longer than that of the $K_v7.3$ and Na_v segments (Fig. 2*C*). Taken together, these data indicate that after sustained M-channel inhibition the rapid forward redistribution of FGF14 and the $K_v7.3$ and Na_v channels occurs at a minutes-to-hours time scale and parallels the adaptive changes in intrinsic excitability. In contrast, the slow ankyrin G relocation matches the hours-to-days time scale characteristic of the adaptive changes in the spontaneous firing rate.

M-Channel Blockade Rapidly Elicits Distal Relocation of AP-Evoked Axonal Na^+ Flux and Shifts the Trigger Zone Away from Soma. To determine the physiological significance of the fast distal shift in Na_v immunofluorescence following sustained M-channel blockade, we used high-speed fluorescence imaging of the Na^+ indicator benzofuran isophthalate (SBFI) to examine the Na^+ dynamics associated with single-spike generation (40, 41). Fast Na^+ imaging acquisition was performed along with whole-cell patch-clamp recordings. The dynamics of Na^+ transients for brief times were previously described in terms of Na^+ influx and lateral diffusion (40, 41). The diffusion effects were minimized by applying only single APs to generate Na^+ transients. We measured the absolute change in fluorescence (ΔF), which is proportional to the Na^+ influx per unit membrane area and is rather unaffected by the somatic light scattering and background tissue fluorescence. The proximal axon was identified as the only process in the cell that possessed sharply rising and rapidly decaying Na^+ transients (*Experimental Procedures*). Following 4 h of XE991 treatment, the location of the peak Na^+ influx was distally shifted from the soma by about 8.8 ± 3.9 μm (untreated: $n = 15$; XE991-treated: $n = 15$) (Fig. 3*A*). Furthermore, although the start of the Na^+ influx was located at approximately the same position from the soma (~12.1 ± 2.4 μm; untreated: $n = 19$; XE991-treated: $n = 16$), the distribution of the Na^+ influx in XE991-treated neurons was significantly wider by about 9.7 ± 3.4 μm (untreated: $n = 19$; XE991-treated: $n = 16$), spreading toward the distal AIS boundary (Fig. 3*A* and Movie S1). By monitoring the changes in the Na^+ influx pattern before and after XE991 exposure to the same hippocampal neuron, we found that the onset of adaptive changes occurred rapidly, within less than 1 h. After not more than 15–45 min of XE991 treatment, significant changes in the AIS sodium transient pattern were noticed in neurons, with a wider distribution of Na^+ influx (36.9 ± 2.2 μm versus 32.5 ± 1.4 μm; $n = 12$) and a distal shift of about 3.4 μm in its maximal value (Fig. 3*B*). Control experiments showed that these parameters did not change during similar periods of recording in the absence of XE991, ruling out possible artifacts caused by cytoplasmic dialysis, metabolic exhaustion, or SBFI diffusion (Fig. S6).

In view of the distal shift of the AIS Na_v immunofluorescence and of Na^+ fluxes, we hypothesized that sustained M-channel blocker exposure would lead the cultured hippocampal neurons to exhibit a distal relocation of the AP trigger zone. To probe this prediction, Na^+ fluxes reported by SBFI fluorescence and spatiotemporal dynamics of AP initiation were measured simultaneously using dual-patch soma–axon recordings as reported previously (40, 41). A whole-cell somatic patch pipette was used to trigger single APs and to dialyze the SBFI probe, thereby allowing identification of the axon among other processes emerging from soma, while a loose patch pipette was used to record action currents at various locations along the AIS. As in cortical pyramidal neurons (40), the amplitude of the action currents decreased as a function of the distance from the soma. The arrowheads in Fig. 4*A*, *Upper* show the normalized action currents recorded from different locations along the proximal axon, revealing the differences in the times of their respective onsets relative to the delayed occurrence of the somatic spike. The AP trigger zone, defined as the site with the longest lag time to somatic signal, shifted distally by 6.3 ± 2.1 μm (untreated: $n = 20$; XE991-treated: $n = 17$) away from the soma in neurons exposed to XE991 for 4 h (Fig. 4). Importantly, comparison of the distances measured from the soma to the site of the maximum Na^+ influx (ΔF max) and to the trigger zone indicated that there was a spatial mismatch between the Na^+ flux and spike

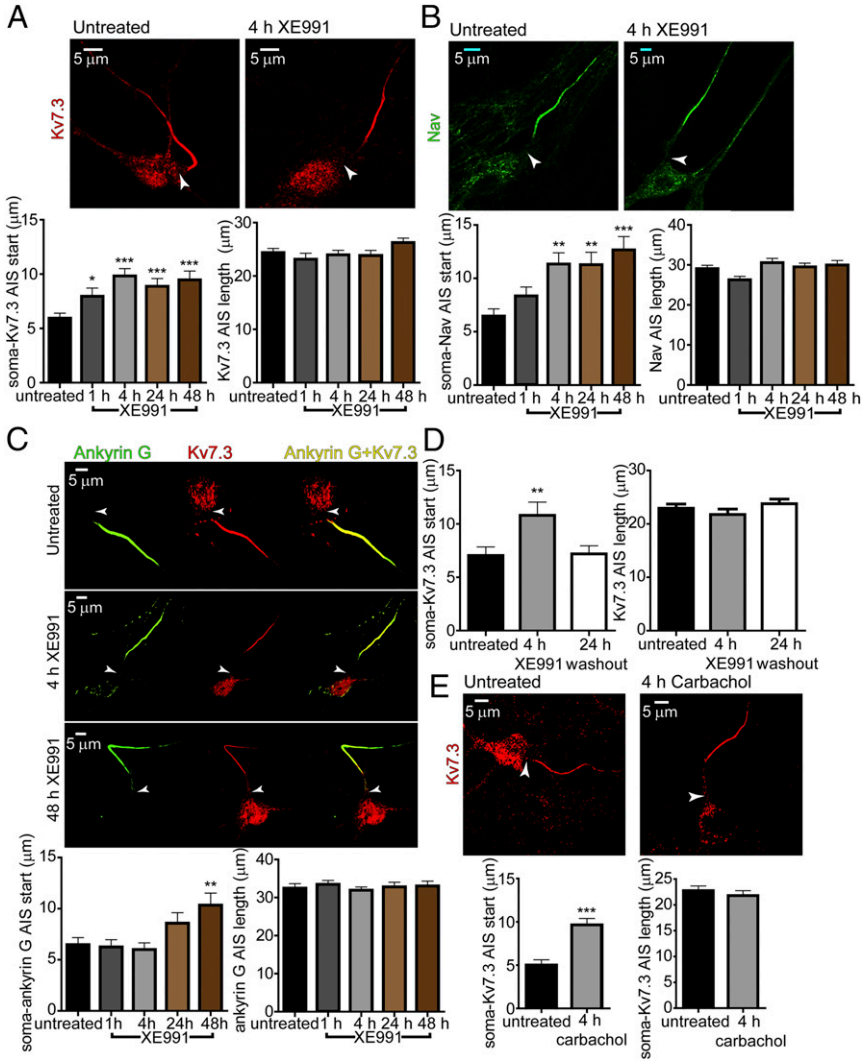

Fig. 2. M-channel inhibition triggers a fast distal shift of AIS Na_v and $K_v7.3$ channels but a slow distal relocation of ankyrin G. (*A*, *Upper*) Representative $K_v7.3$ immunostaining of an untreated neuron (*Left*) and a neuron exposed for 4 h to 10 μM XE991 (*Right*). (*Lower Left*) The $K_v7.3$ segment is significantly shifted distally. The distances from the soma to the start of the $K_v7.3$ label after the indicated duration of XE991 exposure are significantly different from untreated (one-way ANOVA: $*P < 0.05$, $***P < 0.001$, F = 6.523 df = 4, and post hoc Tukey's multiple comparison test) for untreated ($n = 133$) vs. 4-h XE991 treatment ($n = 111$), untreated vs. 24-h XE991 treatment ($n = 95$), and untreated vs. 48 h XE991 treatment ($n = 93$) but not for untreated vs. 1 h ($n = 73$). (*Lower Right*) The length of the $K_v7.3$ segment in the AIS does not change significantly throughout XE991 exposure: untreated ($n = 129$), 1 h ($n = 71$), 4 h ($n = 113$), 24 h ($n = 88$), and 48 h ($n = 90$): one-way ANOVA, $P = 0.2024$, F = 1.495 df = 4. (*B*, *Upper*) Representative Na_v immunostaining of an untreated neuron (*Left*) and a neuron exposed for 4 h to 10 μM XE991 (*Right*). (*Lower Left*) The Na_v segment is shifted distally. The distances from the soma to the start of the Na_v label after the indicated duration of XE991 exposure are significantly different from untreated (one-way ANOVA, $**P < 0.01$, $***P < 0.001$, F = 6.341 df = 4; and post hoc Tukey's multiple comparison test: significantly different for untreated ($n = 99$) vs. 4 h ($n = 91$), untreated vs. 24 h ($n = 95$), and untreated vs. 48 h ($n = 87$); for 1 h ($n = 71$). (*Lower Right*) The length of the Na_v segment in the AIS does not change significantly throughout XE991 exposure: untreated ($n = 98$), 1 h ($n = 63$), 4 h ($n = 90$), 24 h ($n = 94$) and 48 h ($n = 84$): one-way ANOVA, $P = 0.0547$, F = 2.338 df = 4. (*C*, *Upper*) Coimmunolabeling of $K_v7.3$ and ankyrin G in untreated, 4-h XE991-treated, and 48-h XE991-treated neurons. Each row shows the label of ankyrin G alone, $K_v7.3$ alone, and their merging. (*Lower Left*) The ankyrin G segment slowly relocates away from the soma, and the distance reaches significance only at 48 h of XE991 treatment: untreated ($n = 91$), 1 h ($n = 79$), 4 h ($n = 107$), 24 h ($n = 71$), 48 h ($n = 99$): one-way ANOVA, $**P = 0.0008$, F = 4.844 df = 4, and post hoc Tukey's multiple comparison test: significantly different for untreated vs. 48 h. (*Lower Right*) The ankyrin G segment length does not change throughout chronic XE991 exposure: untreated ($n = 90$), 1 h ($n = 76$), 4 h (n = 107), 24 h ($n = 71$), and 48 h ($n = 82$), one-way ANOVA, $P = 0.8801$, F = 0.2967 df = 4. (*D*) Washout of the $K_v7.3$ segment distal shift. After 4 h of XE991 exposure, the medium was replaced by XE991-free medium. (*Left*) The distance between the soma and the start of the $K_v7.3$ segment 24 h after washout was similar to that for untreated neurons: one-way ANOVA, $**P = 0.0087$, F = 4.836 df = 2, and post hoc Tukey's multiple comparison test: significantly different for untreated ($n = 86$) vs. XE991-treated ($n = 61$); not significantly different for untreated vs. washout ($n = 93$). (*Right*) XE991 washout did not change the length of the $K_v7.3$ segment in AIS. (*E*, *Upper*) Representative $K_v7.3$ immunostaining of an untreated neuron and a neuron exposed for 4 h to 10 μM carbachol. (*Lower Left*) The $K_v7.3$ segment is significantly shifted distally. The distances from the soma to the start of the $K_v7.3$ label after 4-h carbachol exposure ($n = 51$) are significantly different from those in the untreated neuron ($n = 54$) (two-tailed unpaired *t* test: $***P < 0.0001$, $t = 4.918$ df = 103). (*Lower Right*) The length of the $K_v7.3$ segment in the AIS does not change significantly following carbachol exposure; untreated, $n = 52$, carbachol, $n = 51$.

initiation in both control (14.4 μm) and XE991-treated (12.2 μm) neurons. In line with the immunofluorescence labeling, the data indicate that protracted M-channel blockade triggered a fast compensatory distal shift in the physical location of $K_v7.3$ and Na_v channels as well as in the trigger zone along the AIS.

Hippocampal CA1 Pyramidal Neurons Adapt Rapidly to Sustained M-Current Inhibition. To confirm the data obtained in cultured hippocampal neurons, whole-cell recordings were done in CA1 pyramidal neurons in acute hippocampal slices. Stable recording could be obtained from the same cell for up to 3 h with no change in the

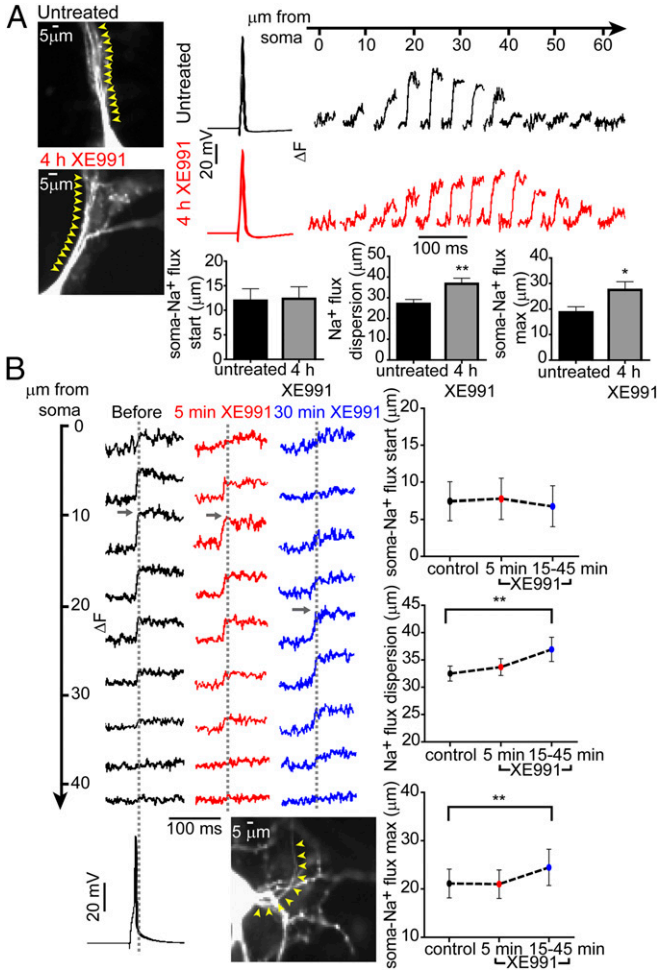

Fig. 3. M-channel blockade rapidly elicits distal relocation of AP-evoked axonal Na^+ flux. (*A*, *Left*) Images of an untreated neuron and a neuron exposed to XE991 for 4 h. Cells were patch-clamped and filled with SBFI. In the whole-cell configuration, a single AP was evoked, and Na^+ imaging was performed simultaneously. Five-micrometer sections along the axon were selected, and changes in Na^+ fluxes were tracked along these sections (yellow arrowheads). (*Upper Right*) Na^+ imaging records from the neurons at the left; single APs induced a bell-shaped increase in Na^+ flux changes along the AIS. (*Lower Right*) The distance between the soma and the start of Na^+ flux changes did not change significantly between untreated neurons ($n = 19$) and neurons chronically treated with XE991 ($n = 16$). The dispersion of Na^+ flux changes along the axon increased significantly after chronic XE991 treatment (two-tailed unpaired *t* test: $^{**}P = 0.0072$, $t = 2.867$, df = 33). Moreover, the location of the peak Na^+ flux changes was distally shifted away from the soma in neurons chronically treated with XE991 compared with untreated neurons (two-tailed unpaired *t* test: $^{*}P = 0.0305$, $t = 2.279$, df = 28). (*B*, *Upper Left*) Representative Na^+ flux change was tracked during XE991 exposure on the same cell. Na^+ imaging was monitored every 5–10 min after XE991 application. The traces show Na^+ flux changes along the AIS before XE991 exposure and after 5 min and 30 min of XE991 exposure. (*Lower Left*) Fast Na^+ transients in the AIS were evoked by somatic single APs using a whole-cell patch-clamp electrode filled with SBFI. Each trace is a mean of the Na^+ imaging intensity in an ∼5-μm-long section along the axon (yellow arrowheads). (*Top Right*) The distance between the soma and the start of the Na^+ transients did not change (control, $n = 18$; 5 min, $n = 18$; 15–45 min, $n = 12$). (*Middle Right*) The dispersion of Na^+ transients in the axon became significantly wider during prolonged XE991 exposure [two-tailed paired *t* test, control vs. 15–45 min ($n = 12$): $^{**}P = 0.0013$, $t = 4.296$, df = 11]. (*Bottom Right*) The peak Na^+ flux changes significantly shifted away from the soma during prolonged XE991 exposure [two-tailed paired *t* test, control vs. 15–45 min ($n = 12$): $^{**}P = 0.0087$, $t = 3.181$, df = 11].

RMP, the threshold current, the frequency of evoked spike discharge, or the delay between the axonal and somatic phases of an upstroke of the somatic spike (Fig. S7). As expected, acute XE991 exposure (5 min) significantly depolarized the RMP, decreased the threshold current, and increased the rate of evoked spike discharge (Fig. 5 *A* and *B*). However, extended incubation with XE991 led to rapid adaptive changes (after 1–3 h) that progressively rescaled the intrinsic excitability values to those of untreated neurons (Fig. 5 *A*

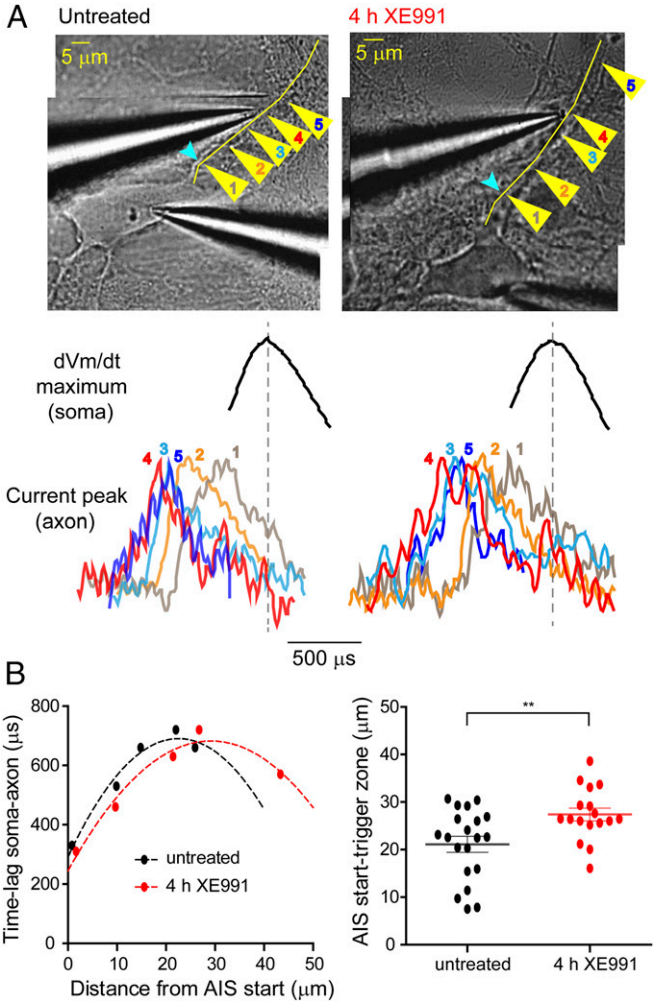

Fig. 4. Distal shift of the axonal trigger zone following prolonged M-channel inhibition. (*A*, *Upper*) Representative superimposed images of an untreated neuron and a neuron treated with XE991 for 4 h and patch-clamped in the whole-cell configuration. The yellow arrowheads show the locations along the axon (1–5) where axonal action currents evoked by single somatic APs were recorded in the loose-patch configuration. The yellow line shows the track of the axon that was detected by SBFI Na^+ imaging before dual-patch recordings. Light blue arrowheads show the start of the AIS (detected by SBFI-detected Na^+ imaging). (*Lower*) Axonal action current normalized to the same amplitude and somatic dV_m/dt maximum peak derived from triggered somatic APs. Somatic and axonal recordings were performed simultaneously at locations 1–5 along the axon. Location 4 (red) is the point where the delay between the axonal and somatic peaks was the largest, indicating that this point is on the trigger zone or is the point nearest to the trigger zone. (*B*, *Left*) Graph showing the points in *A*, with the untreated neuron shown in black and the neuron exposed to XE991 for 4 h shown in red. After prolonged XE991 exposure, the maximum lag time between somatic and axonal spike signals occurred farther from the start of the AIS. Dashed curves correspond to second-order polynomial fits. (*Right*) The spike trigger zone in neurons exposed to XE991 for 4 h was distally shifted away from the start of the AIS compared with untreated neurons. The values of the trigger zone were set as the vertex of the fitted curves (two-tailed unpaired *t* test: $^{**}P = 0.0073$ untreated ($n = 20$) vs. 4 h XE991 ($n = 17$), $t = 2.849$, df = 35).

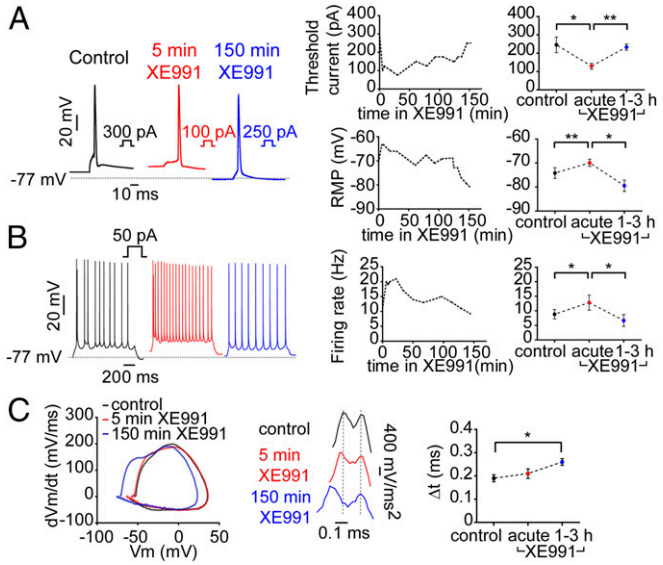

Fig. 5. The intrinsic excitability of CA1 pyramidal neurons from hippocampal slices adapts rapidly during XE991 chronic exposure. (*A*) CA1 pyramidal neurons from hippocampal slices were patch-clamped in the whole-cell configuration. (*Left*) Representative traces of single spikes evoked by 5-ms injection of depolarizing currents in the same cell before (black trace) and after 5 min (red trace) or 150 min (blue trace) exposure to XE991. (*Upper Center*) A representative graph tracking the changes in the threshold current in the same neuron during XE991 exposure. (*Upper Right*) A graph combining data from six different cells. Acute XE991 treatment significantly decreased the threshold current (two-tailed paired *t* test, control vs. acute: $*P = 0.0161$, $n = 6$, $t = 3.568$, df = 5), which returned to a value similar to that of untreated neurons following extended exposure (two-tailed paired *t* test: acute vs. 1–3 h, $**P = 0.0033$, $n = 6$, $t = 5.259$ df = 5). (*Lower Center*) A representative graph tracking the changes of the RMP in the same neuron during XE991 exposure. (*Lower Right*) A graph gathering the data from six different cells. Acute XE991 treatment significantly depolarized the RMP (two-tailed paired *t* test, control vs. acute: $**P = 0.0082$, $n = 6$, $t = 4.235$, df = 5), which repolarized following extended exposure (two-tailed paired *t* test, acute vs. 1–3 h: $*P = 0.0141$, $n = 6$, $t = 3.694$, df = 5). (*B*, *Left*) Representative traces of spike discharge evoked by 1-s injection of 50 pA depolarizing current in the same cell before (black trace) and after 5 min (red trace) or 150 min (blue trace) of XE991 exposure. (*Center*) Tracking of the spike discharge rate in the same neuron during XE991 treatment. (*Right*) Graph gathering the data from six different cells. Acute XE991 treatment significantly increased the evoked spike discharge rate (two-tailed paired *t* test, control vs. acute: $*P = 0.0269$, $n = 6$, t = 3.098, df = 5) and decreased it back following prolonged exposure (two-tailed paired *t* test, acute vs. 1–3 h: $*P = 0.0394$, $n = 6$, $t = 2.769$ df = 5). (*C*, *Left*), phase plots of the first derivative (dV_m/dt) against the membrane potential generated from the representative spikes seen in *A*, *Left*, before (black trace) and after 5 min (red trace) or 150 min (blue trace) of XE991 exposure. (*Center*) Second derivative (dV_m/dt^2) of the same spikes seen on the *Left* emphasizes the remoteness in time between the AIS and somatic phases of APs upstrokes following prolonged XE991 exposure. (*Right*) The lag times collected from six different cells between the AIS and somatic phases derived from the second derivative of single APs before and after XE991 treatment (two-tailed paired *t* test, control vs. 1–3 h: $*P = 0.0189$, $n = 6$, $t = 3.416$, df = 5).

and *B*). Phase plots of evoked single spikes unveiled the two phases of the somatic AP, the early one reflecting the axonal upstroke phase and the later one reflecting the voltage-dependent recruitment of the somatic Na^+ channels (42). The phase-plot pattern was not significantly affected by acute XE991 exposure. Interestingly, prolonged treatment with the M-current blocker changed the phase-plot characteristics by shifting the spike threshold to more negative voltages and by lengthening the interval between axonal and somatic derivative of membrane voltage by time (dV_M)/dt peaks (Fig. 5*C*). The delay between the axonal and the somatic phases, which is further highlighted by analyses of the second derivative of the voltage, increased throughout XE991 exposure (Fig. 5*C*). The homeostatic process may also involve the recruitment of other potassium channels such as $K_v1.1$, $K_v1.2$, $K_v1.4$, and $K_v2.2$ (11), which could account for the overshoot of the threshold potential and the RMP toward negative voltages.

Immunostaining of CA1 pyramidal neurons under control conditions revealed that, as in cultured hippocampal neurons, the proximal boundary of ankyrin G, $K_v7.3$, and Na_v immunofluorescence started at approximately the same location from the soma, but the distal end of the $K_v7.3$ label was consistently shorter than that of Na_v, which itself was shorter than that of ankyrin G. Similarly, after 4-h exposure of hippocampal slices to XE991, the AIS $K_v7.3$ and Na_v segments of CA1 pyramidal neurons were shifted away from the soma by 3.4 ± 0.3 μm (untreated: $n = 201$; 4 h XE991-treated: $n = 193$) and 3.9 ± 0.4 μm (untreated: $n = 156$; XE991-treated for 4 h: $n = 129$), respectively, while ankyrin G was not (Fig. 6). The total length of $K_v7.3$, Na_v, and ankyrin G distributions in the AIS remained the same throughout the XE991 treatment. Together, these data indicate that CA1 pyramidal neurons in slices, similar to hippocampal neurons in culture, undergo rapid homeostatic changes in their intrinsic excitability in response to sustained M-channel inhibition (at a dozens-of-minutes timescale), which are associated with the distal relocation of $K_v7.3$ and Na_v channels and the spike trigger zone away from soma.

Inhibition of CK2 Prevents the Adaptive Changes in Intrinsic Excitability and in the Distal Redistribution of $K_v7.3$ and Na_v Channels Along the AIS. To explore the mechanisms underlying the rapid homeostatic changes, we first used AIS $K_v7.3$ immunostaining as a readout to

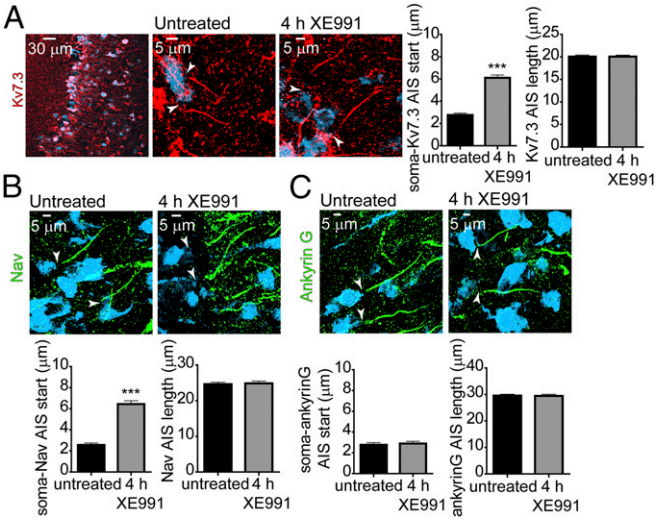

Fig. 6. M-channel inhibition in CA1 hippocampal neurons triggers a fast distal shift of AIS Na_v and $K_v7.3$ channels but not ankyrin G. (*A*, *Left*) $K_v7.3$ and NeuN immunolabeling of CA1 pyramidal neurons from a hippocampal slice at low magnification. (*Center*) $K_v7.3$ and NeuN immunolabeling of untreated CA1 pyramidal neurons and neurons chronically exposed to XE991 (4 h) at higher magnification. (*Right*) The $K_v7.3$ segment in the AIS significantly shifted away from the soma following XE991 treatment [two-tailed unpaired *t* test, untreated ($n = 201$) vs. XE991 ($n = 193$): $***P < 000.1$, $t = 11.27$, df = 392], whereas its length did not change. (*B*, *Upper*) Na_v and NeuN immunolabeling of untreated CA1 hippocampal neurons and CA1 pyramidal neurons chronically exposed to XE991 (4 h). (*Lower*) The Na_v segment in the AIS significantly shifted away from the soma following XE991 treatment [two-tailed unpaired *t* test, untreated ($n = 156$) vs. XE991 ($n = 129$): $***P < 000.1$, $t = 10.83$ df = 283], whereas its length did not change. (*C*, *Upper*) Ankyrin G and NeuN immunolabeling of untreated CA1 pyramidal neurons and CA1 pyramidal neurons chronically exposed to XE991 (4 h). (*Lower*) The AIS ankyrin G segment did not redistribute away from the soma after 4 h of XE991 exposure [two-tailed unpaired *t* test: not significantly different in untreated ($n = 159$) vs. XE991-treated ($n = 143$) neurons, $P = 0.6852$, $t = 0.4058$ df = 300], and its length remained the same.

screen the impact of various drugs on the channel distal shift after the 4-h exposure of cultured hippocampal neurons to 10 μM XE991. The inhibition of protein synthesis, L-type calcium channels, and tyrosine kinases with cycloheximide (30 μM), nifedipine (1 μM), and tyrphostin 25 (10 μM), respectively, when added to XE991 did not preclude the distal relocation of the K_v7.3 segment (Fig. 7*A*). In contrast, two different CK2 inhibitors, 4,5,6,7-tetrabromo-2-azabenzimidazole (TBB) (10 μM) and tetrabromocinnamic acid (TBCA) (25 μM), completely prevented the distal shift of K_v7.3. None of the drugs affected either the length of the K_v7.3 segment or the distance from the soma (Fig. 7*A*). Inhibition of CK2 by TBB also precluded the distal relocation of Na_v channels after prolonged M-channel blockage (Fig. 7*B*). Previous studies showed that AIS sodium channel density is reduced by CK2 inhibition (43). Accordingly, TBB treatment per se significantly increased the threshold current, hyperpolarized the RMP, and decreased the mean firing rate of evoked spike discharge compared with untreated neurons (Fig. 7*C* and Fig. S8). Importantly, inhibition of CK2 by TBB prevented the homeostatic adaptation caused by prolonged M-current inhibition, because it caused the XE991 acute effects on intrinsic excitability, including decreased threshold current and AP amplitude, depolarized RMP, and an increase in the evoked spike discharge rate, to persist over long time periods (Fig. 7*C* and Fig. S8). These results indicate that the homeostatic changes in AIS induced by sustained M-current inhibition were independent of L-type Ca^{2+} channel activity but were contingent on the crucial AIS component, protein kinase CK2. Recent studies suggest that CK2 leads to microtubule destabilization and stimulates microtubule dynamics by increasing the activity of the tubulin deacetylase HDAC6 (44–46). Thus, we checked the impact of 100 nM taxol, a microtubule stabilizer, on the distal redistribution of FGF14 induced by 4 h of XE991 exposure. Taxol inhibited the distal relocation of FGF14 and therefore prevented the plastic adaptive changes (Fig. 7*D*).

Implications of Na^+ and M-Channel Relocation for Spike Generation. An earlier study revealed that activity-dependent relocation of the AIS away from the soma of cultured hippocampal neurons causes a reduction in excitability (32). The mechanism proposed by Grubb and Burrone (32), however, was based primarily on the expectation

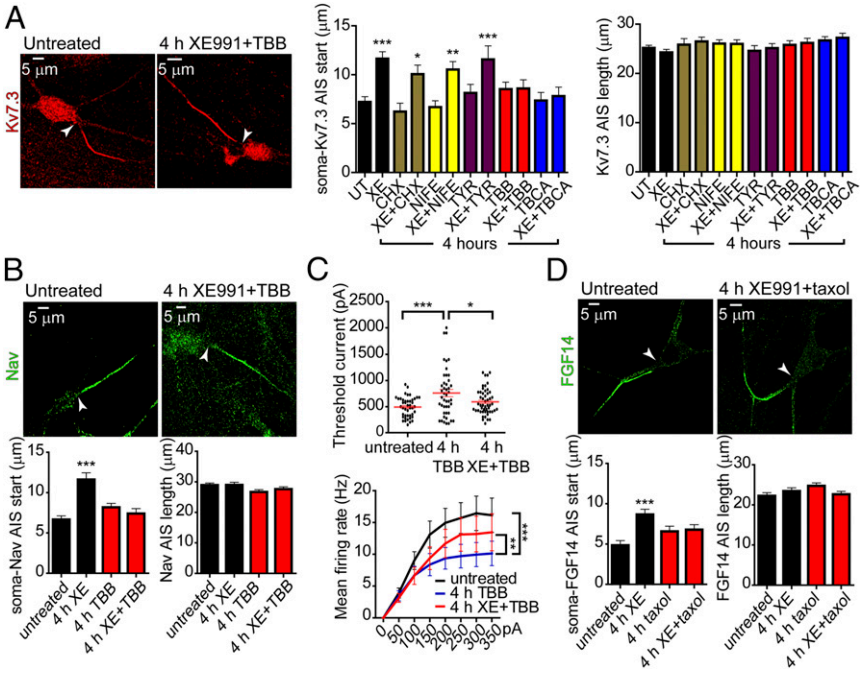

Fig. 7. Inhibition of CK2 prevents the adaptive changes in intrinsic excitability and in the distal shift of K_v7.3 and Na_v channels along the AIS of cultured hippocampal neurons. (*A*, *Left*) K_v7.3 immunostaining of an untreated neuron and a neuron chronically exposed to 10 μM XE991 together with 10 μM TBB (a CK2 inhibitor) for 4 h. (*Center*) Several blockers were added together with XE991 (XE) for 4 h; 30 μM cycloheximide (CHX, a protein synthesis inhibitor), 1 μM nifedipine (NIFE, an L-type calcium channel blocker), and 10 μM tyrphostin 25 (TYR, a tyrosine kinase inhibitor) did not affect the distal shift caused by prolonged M-current inhibition. TBB (10 μM) or TBCA (25 μM), two different CK2 inhibitors, prevented the distal shift promoted by extended XE991 treatment. Untreated (UT), $n = 218$; XE, $n = 191$; CHX, $n = 51$; XE+CHX, $n = 84$; NIFE, $n = 135$; XE+NIFE, $n = 138$; TYR, $n = 78$; XE+TYR, $n = 104$; TBB, $n = 109$; XE+TBB, $n = 103$; TBCA, $n = 99$; XE+TBCA, $n = 90$. One-way ANOVA, $P < 0.0001$, F = 5.286, df = 11, and post hoc Tukey's multiple comparison test: significantly different for CHX vs. XE+CHX (*$P < 0.05$); NIFE vs. XE+NIFE (**$P < 0.01$), and UT vs. XE and TYR vs. XE+TYR (***$P < 0.001$). (*Right*) None of the treatments with the different blockers affected the length of the AIS K_v7.3 segment. (*B*, *Upper*) Na_v immunostaining of untreated neurons and neurons chronically exposed to 10 μM XE991 together with 10 μM TBB for 4 h. (*Lower Left*) The CK2 inhibitor TBB prevented the distal shift of AIS Na_v channels promoted by extended XE991 treatment. Untreated: $n = 175$, XE991: $n = 127$, TBB: $n = 138$, XE+TBB: $n = 125$. One-way ANOVA: ***$P < 0.0001$, F = 13.06, df = 3, and post hoc Tukey's multiple comparison test: significantly different for untreated vs. XE, XE vs. XE+TBB, and XE vs. TBB. (*Lower Right*) The length of the AIS Na_v segment remained unchanged. (*C*, *Upper*) Four-hour TBB exposure alone increased the threshold current. Treatment with XE991+TBB for 4 h decreased the threshold current compared with that obtained with TBB alone. One-way ANOVA: *$P < 0.05$, ***$P = 0.0005$, F = 7.953, df = 2, and post hoc Tukey's multiple comparison test: significantly different for untreated ($n = 44$) vs. TBB ($n = 45$) and TBB vs. TBB+XE ($n = 51$). (*Lower*) Four-hour TBB exposure alone decreased the rate of evoked spike discharge. Four-hour treatment with XE991+TBB increased the evoked spike discharge rate compared with that obtained with TBB alone (untreated: $n = 46$; 4-h TBB treatment: $n = 47$; 4-h XE+TBB treatment: $n = 51$; repeated-measures ANOVA: $P < 0.001$, F = 342.409, df = 1; post hoc Bonferroni comparison test: untreated vs. 4-h TBB treatment, ***$P < 0.001$; 4-h TBB treatment vs. 4-h XE+TBB treatment, **$P = 0.005$). (*D*, *Upper*) FGF14 immunostaining of an untreated neuron and a neuron chronically exposed to 10 μM XE991 together with 100 nM taxol for 4 h. (*Lower Left*) Taxol prevented the distal shift of AIS FGF14 promoted by extended XE991 treatment. Untreated, $n = 99$; XE991, $n = 117$; taxol, $n = 121$; XE+taxol, $n = 106$. One-way ANOVA: ***$P < 0.0005$, F = 6.09, df = 3; and post hoc Tukey's multiple comparison test: significantly different for untreated vs. XE. (*Lower Right*) The length of the AIS FGF14 segment remained unchanged.

of greater passive attenuation of the voltage transients on the way from the soma to the trigger zone enriched by Na^+ channels. On the contrary, our previous evidence based on measurements of the axonal Na^+ fluxes and computational modeling suggested that at any realistic axoplasm resistivity values the relocation of Na^+ channels alone further down the axon could not, by itself, be the reason for a decrease in neuronal excitability (40, 41). However, the rapid M-channel–triggered plasticity described above entails the simultaneous relocation of both Na_v and K_v7 channels (Fig. 8*A*). We therefore tested the idea that this experimentally observed redistribution of the K_v7 conductance within the AIS could be sufficient to suppress spike generation. Using compartmental simulations (27, 47, 48), we examined the effects of varying the AIS position relative to the cell body in models in which only the AIS contained Na_v and K_v7 channels whereas the rest of the neuronal membrane remained passive. In the models, Na^+ channel density was kept constant (2,000 pS/μm^2) while the M-current conductance varied between 0 and 666 pS/μm^2. Relocation of the AIS containing only Na^+ channels away from the soma caused a significant decrease in current threshold (Fig. 8 *B* and *C*) as a result of increased isolation from the capacitive load of the somatodendritic compartment, and the proximal relocation of the AIS had the opposite effect. In models in which the AIS contained both Na^+ and M-channels, however, the effect of AIS relocation was opposite: more current was required to generate an AP with increasing distance between the soma and the AIS proximal edge (Fig. 8 *B* and *C*). We next sought to understand the role of the position of the M-current source within the AIS in spike initiation by constructing models with the AIS shifted either toward or away from the soma by 5 μm (Fig. 8*D*). In both models, increasing K_v7 conductance (gK_v7) while keeping Na conductance (gNa) constant caused a significant increase in spike current threshold. The slope of the threshold relationship (the gK_v7/gNa ratio), however, was significantly steeper for the AIS in a more distal position. Thus, our evidence indicates that, within the AIS, the more distally located K_v7 channels are more effective in suppressing neuronal excitability than those located more proximally.

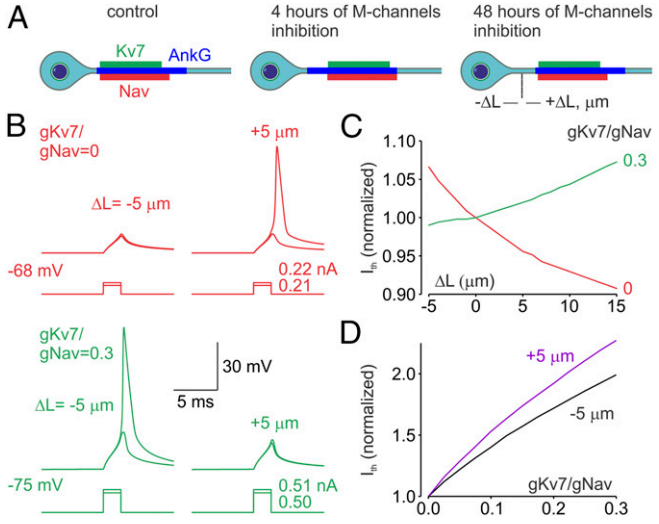

Fig. 8. Functional implications of the distal relocation of the Na_v and K_v7 channels. (*A*) Schematic drawing of the effect of short- and long-term M-channel inhibition on the distribution in the AIS of Na_v (red) and K_v7 (green) channels and ankyrin G (blue). Notice that after relatively short periods of M-channel inhibition the Na_v and K_v7 channels relocate away from the soma [relocation (ΔL) is expressed in micrometers]. This rapid channel relocation readjusts neuronal excitability. If M-channel inhibition persists for days, the ankyrin G segment also relocates away from the soma. (*B*) Simultaneous distal relocation of the AIS Na_v and K_v7 channels causes a decrease in neuronal excitability. (*Upper*) In a model in which 35-μm-long AIS contains Na^+ channels (2,000 pS/μm^2, red traces) but no K_v7 channels, brief somatic current steps with amplitude of less than 0.22 nA fail to elicit an AP following the proximal AIS relocation (ΔL = −5 μm) from the initial position of 10 μm, but they elicit APs following the distal AIS relocation (ΔL = +5 μm). (*Lower*) In a model in which AIS also contains K_v7 channels at density 0.3 times of the Na_v channels (green traces), a current step with an amplitude of 0.51 nA elicits an AP when ΔL = −5 μm, but it fails to do so at ΔL = +5 μm. (*C*) The effect of AIS relocation on current threshold depends on the gK_v7:gNa_v ratio. Distal relocation of the AIS containing only Na^+ channels (gK_v7:gNa_v ratio = 0, red trace) causes a decrease in the current threshold. The current threshold increases as a function of L when the gK_v7:gNa_v ratio is equal to 0.3 (green trace). Shown are the current threshold values normalized to current the threshold for the initial AIS position at distance of 10 μm from the soma (ΔL = 0). (*D*) Varying effects of K_v7 channel density on the current threshold are dependent on the channel position within the AIS. In a model with constant Na^+ channel density, raising gK_v7 is more effective in modulating current threshold when the AIS is relocated away from soma (purple trace, ΔL = +5 μm) than when it is relocated toward the soma (black trace, ΔL = −5 μm).

Discussion

Converging lines of evidence suggest that the AIS is a highly dynamic structure, exhibiting structural plasticity over different timescales ranging from a few hours to several days (7–13, 29–31). Various elegant studies used typical triggers of plasticity such as sensory deprivation, optogenetic stimulation, or high-K^+–induced depolarization (32, 33). Here we triggered AIS plasticity in hippocampal pyramidal neurons by selectively targeting M-channels, which are localized prominently at the AIS and play an important role in tuning neuronal excitability (21, 25, 35, 36). Our evidence indicates that while acute M-current inhibition resulting from cholinergic activation or from direct channel block makes neurons more excitable, longer-lasting (0.5- to 4-h) M-current inhibition elicits an opposite effect, bringing neuronal excitability back toward initial values. This homeostatic compensatory process was faster than that involved in the rescaling of the network spontaneous firing rate, which took 2 d to occur. One could easily appreciate the rapid course of adaptation in CA1 pyramidal neurons, where the changes in intrinsic excitability were recorded from the same cell. The contrasting effects of acute M-channel inhibition with RMP depolarization accompanied by spike amplitude reduction and their subsequent plastic changes underscore the previously suggested dual roles of axonal M-currents (27). On the one hand, AIS M-channels may stabilize the RMP, thereby preventing activation of persistent Na^+ current at subthreshold potentials and dampening spontaneous firing. On the other hand, opening at rest, AIS M-channels may regulate Na_v channel availability by limiting Na_v channel inactivation (27).

The functional and structural changes in the AIS are central to the homeostatic process. Our immunofluorescence-labeling pattern of untreated neurons is somewhat different from previous studies showing that $K_v7.3$ and $K_v7.2$ proteins are weakly detected in or are absent from the proximal AIS in different cell types and that panNa_v AIS staining completely overlaps with that of ankyrin G (13, 21, 27, 43, 49). These discrepancies might be due to differences in cell types, species, strain, or experimental procedures, including the kind of antibodies or fixation conditions. For example, in the avian nucleus magnocellularis neurons, $K_v7.2$ immunoreactivity was distributed along the entire AIS (50). In agreement with our findings and in line with previous work (38, 39), FGF14, which physically bridges the K_v7 and Na_v channels and entirely localizes to the proximal AIS (38, 39), exhibited a shorter length than that of ankyrin G (~24 μm versus 33 μm) in our preparation (Fig. 2*C* and Fig. S5). Immunofluorescence data for CA1 pyramidal neurons in slices and for cultured hippocampal neurons showed that sustained M-channel inhibition induced a rapid distal shift of $K_v7.3$ and Na_v segments with kinetics paralleling the hour-timescale adaptive changes in intrinsic neuronal excitability. The physiological correlate of this distal channel redistribution was provided by monitoring the

changes in the Na^+ flux pattern reported by SBFI Na^+ imaging in the same hippocampal neuron before and after XE991 exposure. Our data indicated that the onset of adaptive changes occurred as early as 15–45 min of XE991 treatment, with a wider distribution of the Na^+ flux and a distal shift in its peak value. Moreover, dual patch soma–axon recording revealed a distal shift in the trigger zone correlating the forward relocation of Na_v channels. The distances measured from the soma to the maximum Na^+ transients (ΔF max) and to the trigger zone revealed a mismatch in location under both control and plasticity conditions, suggesting that this spatial gap is preserved despite the considerable redistribution of Na_v and K_v7 channels. This work reveals correlative homeostatic changes in the spike trigger zone, axonal Na^+ flux, and AIS location of Na_v and K_v7 channels. The similar AIS changes produced by the direct M-channel block and by the sustained cholinergic activation further emphasize the physiological relevance of this homeostatic process in hippocampal pyramidal neurons. Likewise, cholinergic stimulation of muscarinic receptors in the hippocampal dentate gyrus was shown to cause AIS plastic changes in granule cell neurons, which activate Cav3.2, thereby inhibiting M-channels and lowering the AP threshold (26).

Our data reveal differences from the features previously described for AIS plasticity in the nature and timing of the AIS changes as well as in their underlying mechanisms. Grubb and Burrone (32) showed that chronic depolarization with 15 mM K^+ or with optogenetic stimulation moved essential elements of the AIS, including Na_v channels, ankyrin G, βIV spectrin, and FGF14, away from the soma by up to 17 μm. This AIS relocation took 2 d to occur and was correlated with homeostatic alterations in intrinsic neuronal excitability. This distal shift depended on the activation of L-type voltage-gated calcium channels and on related downstream signaling events mediated by the Ca^{2+}-calmodulin–sensitive phosphatase calcineurin (32, 51). In our study, the shift of ankyrin G away from the soma did not occur within this 1-h time-window but instead required 2 d, matching with the time needed to rescale the spontaneous firing rate. Furthermore, the rapid homeostatic changes in the AIS induced by prolonged M-channel inhibition were not dependent on L-type Ca^{2+} channel activity but were contingent on CK2. The significant structural and functional differences in AIS alterations induced by decreased M-channel activity and by high-K^+–induced depolarization/optogenetic stimulation suggest that, depending on the nature of the excitability trigger, different signaling pathways can be mobilized to produce multiple forms of AIS plasticity.

The concomitant distal relocation of Na_v and $K_v7.3$ segments along the AIS suggests that these channels redistribute as a structural and functional unit. In support of this idea, FGF14 was shown to interact with both the $Na_v1.6$ and $K_v7.2$ channels, thereby enabling their bridging in the AIS (38). FGF14 was proposed to be an organizer of $Na_v1.6$ and K_v7 channel localization in the AIS (38). Therefore, it is highly significant that FGF14 exhibited a 4-μm distal shift following 4 h of XE991 treatment without a change in its total length (Fig. S5). This FGF14 distal relocation is like that of the $K_v7.3$ and Na_v channels. Our data suggest that, after M-channel–triggered plasticity, FGF14 undergoes homeostatic changes similar to those of the K_v7 and Na_v channels and support the notion that, thanks to FGF14 bridging, both AIS channels control neuronal excitability as one functional unit.

While blockers of protein synthesis, tyrosine kinases, and L-type calcium channels did not prevent the distal shift of $K_v7.3$ channels, inhibition of CK2 by TBB or TBCA precluded the distal shift of $K_v7.3$ and Na_v channels in the AIS and the rapid adaptive changes in intrinsic excitability. CK2 exerts complex pleiotropic actions in the AIS (1). CK2 phosphorylates Na_v and $K_v7.2/3$ channels to increase their affinity to ankyrin G (22, 43). Therefore, it is possible that CK2 inhibition will prevent the insertion of new $K_v7.2/3$ channels at the distal AIS boundary without affecting those already stably anchored to ankyrin G at the proximal boundary. Thereby, CK2 may prevent the distal relocation observed after prolonged M-channel inhibition (2). CK2 phosphorylates calmodulin to increase its interaction with $K_v7.2$ subunits, an effect that may be crucial for AIS targeting of $K_v7.2/3$ (52, 53), with the same consequences as described above (3). While previous work suggested that CK2 confers microtubule stability (54, 55), recent lines of evidence indicate that CK2 leads to microtubule destabilization and stimulates microtubule dynamics by increasing the activity of the tubulin deacetylase HDAC6. CK2 was shown to increase HDAC6 activity either by direct HDAC6 phosphorylation (46) or by priming GSK3β, which interacts with HDAC6 and enhances its activity by increasing HDAC6 phosphorylation at Ser22 (45). Acetylation of α-tubulin contributes to microtubule stability, and α-tubulin deacetylation via increased HDAC activity was suggested to lead to microtubule instability and cell motility (44, 45). Along this line, a recent work in a mouse model of familial dysautonomia showed that reduced levels of IκB kinase complex-associated protein (IKAP) lead to increased HDAC6 levels in sensory neurons, thereby reducing acetylated α-tubulin and provoking microtubule instability (56). We suggest that the homeostatic changes subsequent to prolonged M-channel inhibition require enhanced microtubule dynamics and instability to produce the distal redistribution of Na_v and K_v7 channels along the AIS. In support of this idea, our data indicate that taxol, a microtubule stabilizer, inhibits the distal relocation of FGF14 and therefore prevents the plastic adaptive changes. Our results are also in line with a recent study showing that taxol could prevent the distal AIS repositioning induced by hyperphosphorylation of the tau protein in an animal model of Alzheimer's disease (57). Together, the data suggest that this rapid and unique form of homeostatic plasticity triggered by alterations in M-channel activity is dependent on CK2 activity and microtubule dynamics.

Experimental Procedures

Animals. BALB/c mice were used for generating the primary cultures of hippocampal neurons and for acute hippocampal slice experiments. All experimental protocols were approved by the Institutional Animal Care and Use Committee of Tel Aviv University, Tel Aviv, (animal welfare authorization number 01-16-012).

Drugs. The following drugs were used: XE991 (Tocris), Carbachol (Sigma), cycloheximide (Sigma), nifedipine (Sigma), Tyrphostin 25 (Sigma), TBCA (Sigma), TBB (Tocris), bicuculline (Sigma), picrotoxin (Sigma), NBQX (Sigma), AP5 (Sigma), tetrodotoxin (Alomone Labs), ZD7288 (Tocris), and 4-aminopyridine (Sigma).

Details of primary cultures of hippocampal neurons, acute brain slice preparation, sodium imaging, electrophysiology, immunostaining, data analysis, statistics, and compartmental modeling are provided in *SI Experimental Procedures*.

ACKNOWLEDGMENTS. We thank Prof. Daniel Gitler and members of his laboratory for their help in providing tissue-culture facilities. This work was supported by Israel Science Foundation (ISF) Grant 1302/14 (to I.A.F.) and by Deutsche Israel Programme Grant DFG-DIP-AT119/1-1 and ISF Grants 2092/14 and 1365/17 (to B.A.), who holds the Andy Libach Professorial Chair in Clinical Pharmacology and Toxicology.

1. Turrigiano G (2012) Homeostatic synaptic plasticity: Local and global mechanisms for stabilizing neuronal function. *Cold Spring Harb Perspect Biol* 4:a005736.
2. Gonzalez-Islas C, Wenner P (2006) Spontaneous network activity in the embryonic spinal cord regulates AMPAergic and GABAergic synaptic strength. *Neuron* 49:563–575.
3. Maffei A, Nelson SB, Turrigiano GG (2004) Selective reconfiguration of layer 4 visual cortical circuitry by visual deprivation. *Nat Neurosci* 7:1353–1359.
4. Marder E, Goaillard JM (2006) Variability, compensation and homeostasis in neuron and network function. *Nat Rev Neurosci* 7:563–574.
5. Turrigiano GG, Nelson SB (2004) Homeostatic plasticity in the developing nervous system. *Nat Rev Neurosci* 5:97–107.
6. Wierenga CJ, Walsh MF, Turrigiano GG (2006) Temporal regulation of the expression locus of homeostatic plasticity. *J Neurophysiol* 96:2127–2133.

7. Adachi R, Yamada R, Kuba H (2015) Plasticity of the axonal trigger zone. *Neuroscientist* 21:255–265.
8. Grubb MS, et al. (2011) Short- and long-term plasticity at the axon initial segment. *J Neurosci* 31:16049–16055.
9. Gründemann J, Häusser M (2010) Neuroscience: A plastic axonal hotspot. *Nature* 465: 1022–1023.
10. Kole MHP, Stuart GJ (2012) Signal processing in the axon initial segment. *Neuron* 73: 235–247.
11. Petersen AV, Cotel F, Perrier JF (2016) Plasticity of the axon initial segment: Fast and slow processes with multiple functional roles. *Neuroscientist* 23:364–373.
12. Yamada R, Kuba H (2016) Structural and functional plasticity at the axon initial segment. *Front Cell Neurosci* 10:250.
13. Yoshimura T, Rasband MN (2014) Axon initial segments: Diverse and dynamic neuronal compartments. *Curr Opin Neurobiol* 27:96–102.
14. Farías GG, Guardia CM, Britt DJ, Guo X, Bonifacino JS (2015) Sorting of dendritic and axonal vesicles at the pre-axonal exclusion zone. *Cell Rep* 13:1221–1232.
15. Leterrier C (2016) The axon initial segment, 50 years later: A nexus for neuronal organization and function. *Curr Top Membr* 77:185–233.
16. Leterrier C, Dargent B (2014) No Pasaran! Role of the axon initial segment in the regulation of protein transport and the maintenance of axonal identity. *Semin Cell Dev Biol* 27:44–51.
17. Leterrier C, et al. (2015) Nanoscale architecture of the axon initial segment reveals an organized and robust scaffold. *Cell Rep* 13:2781–2793.
18. Xu K, Zhong G, Zhuang X (2013) Actin, spectrin, and associated proteins form a periodic cytoskeletal structure in axons. *Science* 339:452–456.
19. Chung HJ, Jan YN, Jan LY (2006) Polarized axonal surface expression of neuronal KCNQ channels is mediated by multiple signals in the KCNQ2 and KCNQ3 C-terminal domains. *Proc Natl Acad Sci USA* 103:8870–8875.
20. Garrido JJ, et al. (2003) A targeting motif involved in sodium channel clustering at the axonal initial segment. *Science* 300:2091–2094.
21. Pan Z, et al. (2006) A common ankyrin-G-based mechanism retains KCNQ and NaV channels at electrically active domains of the axon. *J Neurosci* 26:2599–2613.
22. Xu M, Cooper EC (2015) An ankyrin-G N-terminal gate and protein kinase CK2 dually regulate binding of voltage-gated sodium and KCNQ2/3 potassium channels. *J Biol Chem* 290:16619–16632.
23. Hu W, et al. (2009) Distinct contributions of Na(v)1.6 and Na(v)1.2 in action potential initiation and backpropagation. *Nat Neurosci* 12:996–1002.
24. Van Wart A, Trimmer JS, Matthews G (2007) Polarized distribution of ion channels within microdomains of the axon initial segment. *J Comp Neurol* 500:339–352.
25. Jentsch TJ (2000) Neuronal KCNQ potassium channels: Physiology and role in disease. *Nat Rev Neurosci* 1:21–30.
26. Martinello K, et al. (2015) Cholinergic afferent stimulation induces axonal function plasticity in adult hippocampal granule cells. *Neuron* 85:346–363.
27. Battefeld A, Tran BT, Gavrilis J, Cooper EC, Kole MHP (2014) Heteromeric Kv7.2/7.3 channels differentially regulate action potential initiation and conduction in neocortical myelinated axons. *J Neurosci* 34:3719–3732.
28. Eccles JC, Ito M, Szentagothai J, eds (1967) *The Cerebellum as a Neuronal Machine* (Springer, New York), p 334.
29. Scott RS, et al. (2014) Neuronal adaptation involves rapid expansion of the action potential initiation site. *Nat Commun* 5:3817.
30. Yang S, et al. (2016) β-arrestin-dependent dopaminergic regulation of calcium channel activity in the axon initial segment. *Cell Rep* 16:1518–1526.
31. Yin L, et al. (2017) Selective modulation of axonal sodium channel subtypes by 5-HT1A receptor in cortical pyramidal neuron. *Cereb Cortex* 27:509–521.
32. Grubb MS, Burrone J (2010) Activity-dependent relocation of the axon initial segment fine-tunes neuronal excitability. *Nature* 465:1070–1074.
33. Kuba H, Oichi Y, Ohmori H (2010) Presynaptic activity regulates Na(+) channel distribution at the axon initial segment. *Nature* 465:1075–1078.
34. Evans MD, Dumitrescu AS, Kruijssen DLH, Taylor SE, Grubb MS (2015) Rapid modulation of axon initial segment length influences repetitive spike firing. *Cell Rep* 13: 1233–1245.
35. Brown DA, Adams PR (1980) Muscarinic suppression of a novel voltage-sensitive K+ current in a vertebrate neurone. *Nature* 283:673–676.
36. Shah M, Mistry M, Marsh SJ, Brown DA, Delmas P (2002) Molecular correlates of the M-current in cultured rat hippocampal neurons. *J Physiol* 544:29–37.
37. Brown DA, Hughes SA, Marsh SJ, Tinker A (2007) Regulation of M(Kv7.2/7.3) channels in neurons by PIP(2) and products of PIP(2) hydrolysis: Significance for receptor-mediated inhibition. *J Physiol* 582:917–925.
38. Pablo JL, Pitt GS (2017) FGF14 is a regulator of KCNQ2/3 channels. *Proc Natl Acad Sci USA* 114:154–159.
39. Pablo JL, Wang C, Presby MM, Pitt GS (2016) Polarized localization of voltage-gated Na+ channels is regulated by concerted FGF13 and FGF14 action. *Proc Natl Acad Sci USA* 113:E2665–E2674.
40. Baranauskas G, David Y, Fleidervish IA (2013) Spatial mismatch between the Na+ flux and spike initiation in axon initial segment. *Proc Natl Acad Sci USA* 110:4051–4056.
41. Fleidervish IA, Lasser-Ross N, Gutnick MJ, Ross WN (2010) Na+ imaging reveals little difference in action potential-evoked Na+ influx between axon and soma. *Nat Neurosci* 13:852–860.
42. Hamada MS, Kole MHP (2015) Myelin loss and axonal ion channel adaptations associated with gray matter neuronal hyperexcitability. *J Neurosci* 35:7272–7286.
43. Bréchet A, et al. (2008) Protein kinase CK2 contributes to the organization of sodium channels in axonal membranes by regulating their interactions with ankyrin G. *J Cell Biol* 183:1101–1114.
44. Li L, Yang XJ (2015) Tubulin acetylation: Responsible enzymes, biological functions and human diseases. *Cell Mol Life Sci* 72:4237–4255.
45. Li Y, Shin D, Kwon SH (2013) Histone deacetylase 6 plays a role as a distinct regulator of diverse cellular processes. *FEBS J* 280:775–793.
46. Watabe M, Nakaki T (2011) Protein kinase CK2 regulates the formation and clearance of aggresomes in response to stress. *J Cell Sci* 124:1519–1532.
47. Hines ML, Carnevale NT (1997) The NEURON simulation environment. *Neural Comput* 9:1179–1209.
48. Kole MHP, et al. (2008) Action potential generation requires a high sodium channel density in the axon initial segment. *Nat Neurosci* 11:178–186.
49. Devaux JJ, Kleopa KA, Cooper EC, Scherer SS (2004) KCNQ2 is a nodal K+ channel. *J Neurosci* 24:1236–1244.
50. Kuba H, Yamada R, Ishiguro G, Adachi R (2015) Redistribution of Kv1 and Kv7 enhances neuronal excitability during structural axon initial segment plasticity. *Nat Commun* 6:8815.
51. Evans MD, et al. (2013) Calcineurin signaling mediates activity-dependent relocation of the axon initial segment. *J Neurosci* 33:6950–6963.
52. Cavaretta JP, et al. (2014) Polarized axonal surface expression of neuronal KCNQ potassium channels is regulated by calmodulin interaction with KCNQ2 subunit. *PLoS One* 9:e103655.
53. Kang S, Xu M, Cooper EC, Hoshi N (2014) Channel-anchored protein kinase CK2 and protein phosphatase 1 reciprocally regulate KCNQ2-containing M-channels via phosphorylation of calmodulin. *J Biol Chem* 289:11536–11544.
54. Lim ACB, Tiu SY, Li Q, Qi RZ (2004) Direct regulation of microtubule dynamics by protein kinase CK2. *J Biol Chem* 279:4433–4439.
55. Sanchez-Ponce D, Muñoz A, Garrido JJ (2011) Casein kinase 2 and microtubules control axon initial segment formation. *Mol Cell Neurosci* 46:222–234.
56. Naftelberg S, et al. (2016) Phosphatidylserine ameliorates neurodegenerative symptoms and enhances axonal transport in a mouse model of familial dysautonomia. *PLoS Genet* 12:e1006486.
57. Hatch RJ, Wei Y, Xia D, Götz J (2017) Hyperphosphorylated tau causes reduced hippocampal CA1 excitability by relocating the axon initial segment. *Acta Neuropathol* 133:717–730.